Experiments on excitation of Alfvén eigenmodes by alpha-particles with bump-on-tail distribution in JET DTE2 plasmas

S.E. Sharapov[1], H.J.C. Oliver[1], J. Garcia[2], D.L. Keeling[1], M. Dreval[3], V. Goloborod'ko[4], Ye.O. Kazakov[5], V.G. Kiptily[1], Ž. Štancar[1], P.J. Bonofiglo[6], R. Coelho[7], T. Craciunescu[8], J. Ferreira[7], A. Figueiredo[7], N. Fil[1], M. Fitzgerald[1], F. Nabais[7], M. Nocente[9,10], P.G. Puglia[11], J. Rivero-Rodriguez[1], P. Rodrigues[7], M. Salewski[12], R.A. Tinguely[13], L.E. Zakharov[14], and JET contributors*

[1]UKAEA, Abingdon, United Kingdom
[2]CEA, IRFM, F-13108 Saint-Paul-lez-Durance, France
[3]Institute of Plasma Physics, National Science Center KIPT, Kharkiv, Ukraine
[4]Institute for Nuclear Research, Kiev, Ukraine
[5]Laboratory for Plasma Physics, LPP-ERM/ KMS, TEC Partner, Brussels, Belgium
[6]Princeton Plasma Physics Laboratory, Princeton, NJ, USA
[7]Instituto de Plasmas e Fusao Nuclear, IST, Universidade de Lisboa, 1049-001 Lisboa, Portugal
[8]National Institute for Laser, Plasma and Radiation Physics, Bucharest, Romania
[9]Dipartimento di Fisica 'G.Occhialini', Universit`a di Milano-Bicocca, Milano, Italy
[10]Institute for Plasma Science and Technology, National Research Council, Milan, Italy
[11]EPFL, Swiss Plasma Center, CH-1015 Lausanne, Switzerland
[12]Department of Physics, Technical University of Denmark, Kgs. Lyngby, Denmark
[13]MIT Plasma Science and Fusion Center, Cambridge, USA
[14]Helsinki University, Finland

*See the author list of J. Mailloux et al 2022 Nucl. Fusion **62** 042026 https://doi.org/10.1088/1741-4326/ac47b4

E-mail contact of main author: Sergei.Sharapov@ukaea.uk

Abstract

Dedicated experiments were performed in JET DTE2 plasmas for obtaining an α-particle bump-on-tail (BOT) distribution aiming at exciting Alfvén Eigenmodes (AEs). NBI-only heating with modulated power was used so that fusion-born α-particles were the only ions present in the MeV energy range in these DT plasmas. The beam power modulation on a time scale shorter than the α-particle slowing down time was chosen for modulating the α-particle source and thus sustaining a BOT in the α-particle distribution. High-frequency modes in the TAE frequency range and multiple short-lived modes in a wider frequency range have been detected in these DT discharges with interferometry, soft X-ray cameras, and reflectometry. The modes observed were localised close to the magnetic axis, and were not seen in the Mirnov coils. Analysis with the TRANSP and Fokker-Planck FIDIT codes confirms that α-particle distributions with bump-on-tail in energy were achieved during some time intervals in these discharges though no clear correlation was found between the times of the high-frequency mode excitation and the BOT time intervals. The combined MHD and kinetic modelling studies show that the high-frequency mode in the TAE frequency range is best fitted with a TAE of toroidal mode number n= 9. This mode is driven mostly by the on-axis beam ions while the smaller drive due to the pressure gradient of α-particles allows overcoming the marginal stability and exciting the mode [H.J.C. Oliver *et al*. *Toroidal Alfvén eigenmodes observed in low power JET deuterium-tritium plasmas*, to be submitted to Nuclear Fusion (2023)]. The observed multiple short-lived modes in a wider frequency range are identified as the on-axis kinetic Alfvén eigenmodes predicted in [M.N. Rosenbluth, P.H. Rutherford, Phys. Rev. Lett. **34** (1975) 1428].

1 Introduction

Excitation of Alfvén instabilities by energetic particles including fusion-born α-particles has been long recognized [1, 2] as one of the most important problems for tokamak operations in DT plasmas of burning plasma experiments [3]. The excitation thresholds of energetic particle-driven instabilities are determined by a balance between the wave growth due to resonant interaction with the energetic particles and the wave damping due to background plasma. In order to identify the waves with lowest excitation thresholds, a search for weakly-damped Alfvén eigenmodes (AEs) with low continuum damping started as early as [1]. It was shown in [1] that AEs with essential kinetic Alfvén wave (KAW) [4] structure surrounding the tokamak magnetic axis could exist and be excited by either a radial pressure gradient or a bump-on-tail distribution of energetic particles. In what follows we'll label these on-axis AEs predicted by Rosenbluth and Rutherford as "RR-modes". In parallel, the author of [2] has drawn a vivid concept of an AE excitation with sub-Alfvénic energetic particles (transformed later into $V_{\|} = V_A/3$ resonance for TAEs) assuming that some types of weakly-damped AEs could be found.

It was later established that other types of weakly-damped AEs could exist such as Global AEs [5, 6], Toroidal AEs [7, 8], Elliptical AEs [9, 10] and Alfvén cascades [11]. All these various AEs localized sufficiently far from the magnetic axis attracted most of attention in comparison to RR-modes since the radial pressure gradients of energetic particles typically goes to zero at the magnetic axis and becomes significant from around of a quarter to a half of the plasma radius. In particular, for α-particles with a slowing-down distribution in energy and isotropic in the pitch-angle the free energy source associated with the radial pressure gradient of α-particles was considered as the main driving force for the AEs [5-11]. This free energy source was also a key assumption in interpreting experimental data on Alfvén instabilities and for assessing AE stability in ITER [3].

However, recent JET experiments with D-^{3}He plasmas performed before the DTE2 campaign have exhibited instabilities suggesting that the free energy source was another in addition to the radial pressure gradient only [12]. Further investigation of these observations has shown that the intensity of the source of 3.7 MeV α-particles born in D-^{3}He reactions was modulated by sawteeth with periods shorter than the α-particle slowing-down time, and a bump-on-tail (BOT) distribution moving towards lower energy range could have been sustained in the α-particle distribution under these conditions. This finding of the sustained moving BOT distribution of α-particles, instead of the slowing-down distribution, has shown that amendments are required to the assessment of the

excitation thresholds of AEs in tokamaks since the free energy source associated with the positive slope of the distribution function in energy, $\mathrm{d}F_\alpha/\mathrm{d}E > 0$, can modify the estimate of the drive of AEs by α-particles.

For further investigation of the possibility of obtaining a sustained BOT of α-particle distribution, dedicated experiments were planned and carried out in 2021 with α-particles born in JET DT plasmas during the DTE2 campaign with Be/W wall. The critical question to answer was whether we could, via modulating the power of neutral beam injection (NBI), by using sawteeth, or via some other mechanisms create a BOT distribution of α-particles, which amplifies the AE drive and affects significantly the AE instability zones in burning DT plasmas. The DT experiment performed could be considered as a dedicated step towards answering this question, and the aim of this paper is to describe results of these experiments. Note here that the experiments described in this paper were complementary to the mainstream DTE2 "NBI afterglow" TAE experiments with elevated q-profiles [13].

2 Experimental setup

Since the α-particle BOT observations in D-^{3}He plasmas were made just before the DTE2 campaign and no time remained for preparing in deuterium the specific BOT scenario for the DT case, only DT discharges with relatively low NBI power and limited tritium and neutron budgets were allowed for this experiment during the DTE2. For achieving a BOT distribution of α-particles in JET DT plasmas, a scenario was proposed mimicking the JET D-^{3}He discharges [12] with short-period sawteeth. In this scenario, instead of the sawteeth modulating the source of α-particles in D-^{3}He plasmas, a more predictable and controllable technique was proposed of modulating the α-particle source via modulating NBI power. As the dominant fusion yield in DTE2 discharges was determined by beam-plasma reactions, a modulation of NBI power gave the possibility of a direct and easy way to control modulation of the α-particle source. A Fokker-Plank FIDIT model [14] was employed for optimising the time period and the depth of NBI power modulation required for sustaining a BOT in the α-particle distribution. During the FIDIT modelling, it was found that it is the relative depth of the NBI power modulation rather than the absolute value of the NBI power that plays a main role in the formation of a BOT in the α-particle distribution. For validating this modelling result, a modulation of the beam power in DTE2 discharges was proposed with an increasing relative depth as Figure 1 shows for maximising the BOT formation.

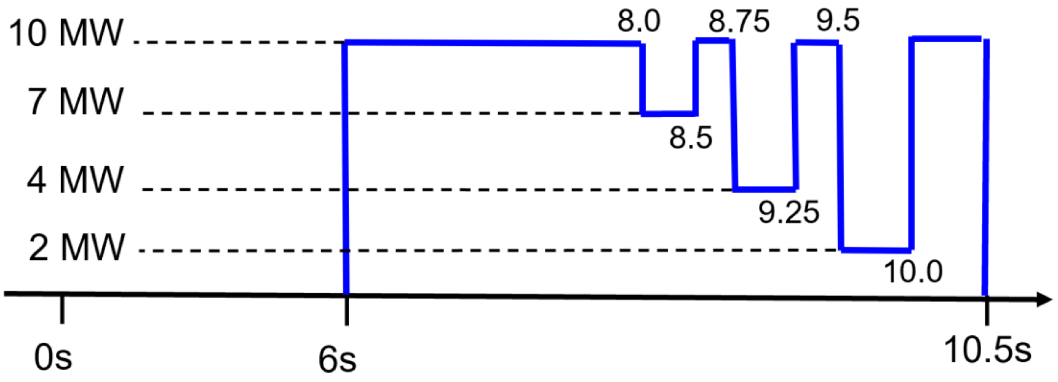

Figure 1. The intended NBI power waveform aiming at a modulation of α-particle source.

In JET with Be/W wall, central ion cyclotron resonance heating (ICRH) was typically used for mitigating core W accumulation. However, it was of principal concern for dedicated α-particle experiments that ICRH could not be employed as ICRH-accelerated fast ions would prohibit a clear identification of α-particle effects. In order to avoid any energetic particle population in the MeV energy range other than fusion-born α-particles, NBI heating with maximum injection energy of ~ 115 keV was employed only in the BOT series of DTE2 discharges. As no reference scenario with NBI-only heating was available to start from, discharges were proposed with a short main heating phase of ~ 4 sec only so the core tungsten accumulation would not cool down the central plasma too much. The pulse type was adopted from a discharge similar to the D-^{3}He reference with safety factor $q(0)$ ~ 1 but without ICRH. Direct measurements of fusion-born lost α-particles were performed with the use of the scintillator probe (SP) and Faraday cups [15]. Mirnov coils and interferometry [16], sweeping frequency reflectometry [17], and soft X-ray (SXR)[18] diagnostics were employed for detecting possible high-frequency modes excited with α-particles.

During the DTE2 campaign, five DT pulses (#99500-99503 and pulse #99627) were performed in the scenario described above, with B_T = 3.7 T, I_P = 2.5 MA, with modulated NBI power and maximum of $P_{NBI} \approx$ 10-15 MW. A pulse with D-beam injected into pure D plasma was performed as a diagnostic reference after the DTE2 campaign (pulse #100797). Each of the DTE2 discharges had a DT neutron yield up to $R_{DT} = 6.5 \times 10^{17}$ s^{-1}. The main source of DT neutrons and α-particles in these discharges was of the beam-plasma type. It was mostly the electron temperature affecting the beam slowing down time, and the beam and plasma D:T compositions that determined the value of the fusion yield. During the experiments, both D and T beams were injected into the five discharges listed above and the plasma deuterium-tritium mixtures varied from D:T = 33:67 (T-rich plasmas) to D:T = 55:45.

3 Injection of T-beam followed by D-beam into JET DT plasma

To start, a discharge has been performed (JET pulse #99500) with T-beam injection followed by D-beam injection into a JET DT plasma with a somewhat higher T concentration than D concentration, D:T≈ 42:58. This was done in order to assess the main characteristics of DT neutrons, α-particles, MHD and fast particle diagnostics, and to compare the beam-plasma fusion rates and the corresponding transport modelling for the two beams with different hydrogen isotopes. Figure 2 shows the temporal evolution of the main physics parameters in this discharge. The rate of DT neutrons displayed in Fig.2 is seen to saturate during the time interval from ~6.3 s to ~7.3 s, together with $T_e(0)$ during the steady-state T-NBI power phase. Then, during the T-NBI power decrease/ modulation interval from ~7.3 s to ~9 s, the neutron rate decreases accordingly, and increases rather quickly when D-NBI is injected at 9 s. The discharge remained in L-mode throughout whole time. The maximum neutron rate of $R_{NT} \approx 3.1 \times 10^{17}$ s^{-1} is achieved during D-beam injection into T-rich plasma at ~9.6 s, in agreement with expected beam-plasma fusion from the different isotopes.

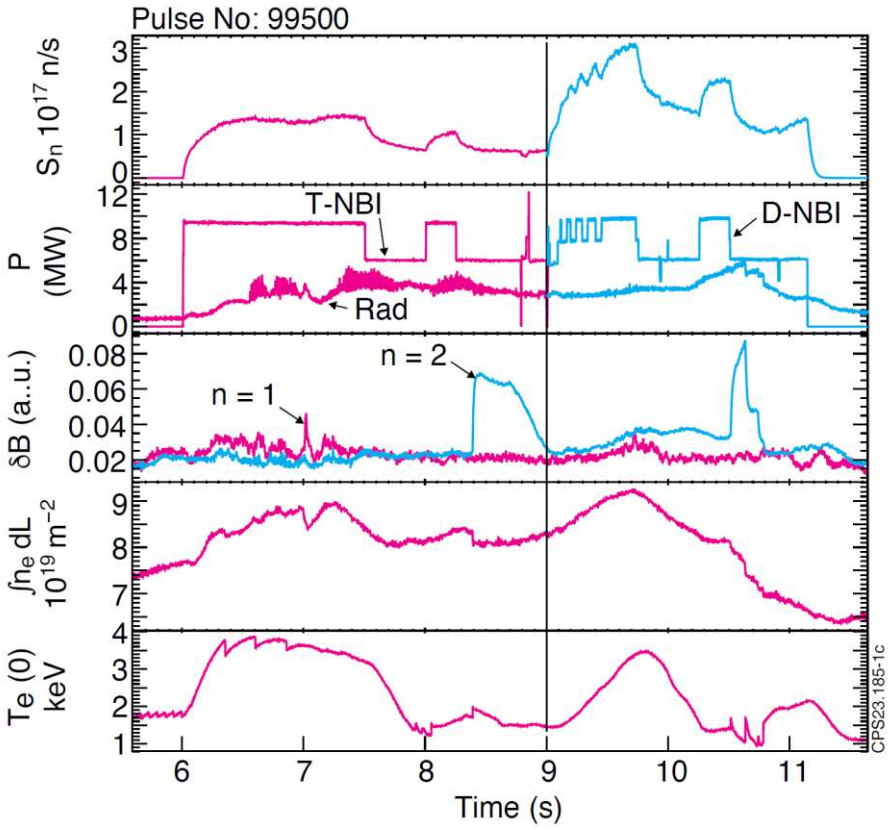

Figure 2 From top to bottom: DT neutron rate in discharge #99500; Power waveforms of T-NBI (till 9 s) and D-NBI (from 9 s) and temporal evolution of plasma radiation; amplitudes of low-frequency n=1 and n=2 MHD perturbations measured with the set of Mirnov coils; electron density integrated

along the vertical line-of-sight through the magnetic axis and measured with high time resolution by interferometry; on-axis electron temperature from ECE measurements.

Losses of energetic particles in these DT discharges were best detected with the scintillator probe (SP). The SP provided a 2D image of the lost ions with their Larmor radii and pitch-angle axes of Figure 3. The observations of the lost energetic ions with Larmor radii in the range ~8–11 cm and pitch-angles in the range ~55^o – 80^o are consistent with losses of fusion-born α-particles as no other energetic ions with such parameters exist in this discharge. Indeed, the Larmor radii of the ions lost agreed well with the value of the magnetic field ~ 2.8 T at the position of SP and with the energy range of ~ 3–4 MeV expected for the α-particle source. It can be seen in Fig.3 that the lost α-particles formed a "double-hump" in their pitch-angles. A backward orbit following procedure has shown that α-particles with their orbit originated from the major raii ~ 2.75 m and ~ 3.6 m have had higher losses than α-particles from the proximity of the magnetic axis at ~ 3.15 m (the magnetic axis was at ~ 3 m). A similar double-hump pitch-angle dependence was observed in SP data during D-beam injection at ~10 s. Possible interpretations of the "double-hump" effect are discussed in [19].

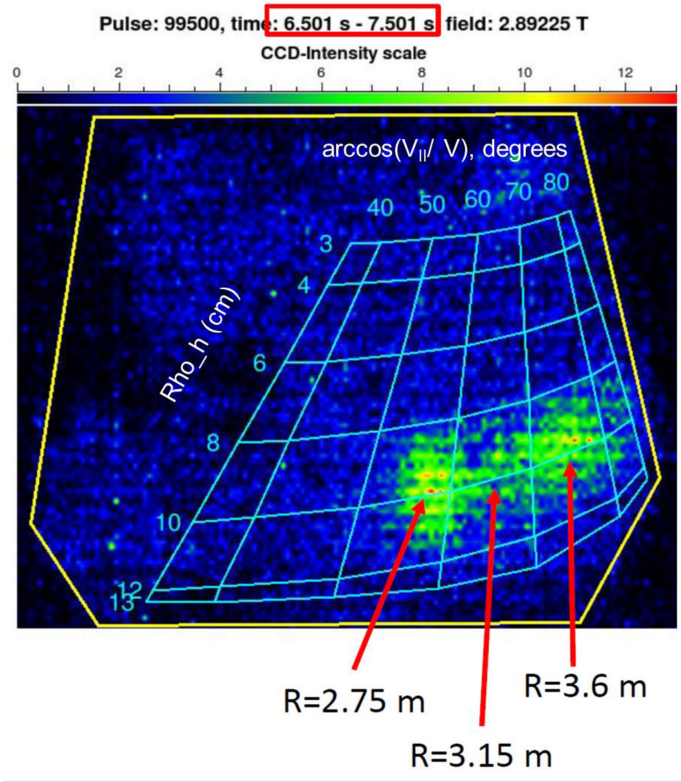

Figure 3. Data from the scintillator probe showing counts of lost α-particles and their pitch-angles and Larmor radii ρ_{hot} (cm) during the time interval 6.5 – 7.5 s in pulse #99500.

The MHD measurements were performed with interferometry [16], reflectometry [17], soft X-ray (SXR) [18], and Mirnov coils [16]. Figure 4 shows the observation of high-frequency modes in the TAE frequency range detected with the sweeping frequency reflectometer. For the magnetic field gradient in this discharge, the sweeping frequency of the reflectometer was probing δn perturbations of the plasma along the major radius of the machine from the magnetic axis at R_0 ~ 3 m to R ~ 3.75 m. Multiple modes seen in the frequency range from ~180 kHz to ~325 kHz during time period from ~7.45 s to ~7.55 correspond to the position of the reflection layer moving from ~3.25 m to ~3.15 m thus showing the core localisation of the modes.

The time of the observations corresponds to the time interval of α-particle measurements in Fig.3. The modes are not seen in Mirnov coils thus excluding identification of their toroidal mode numbers. In the mode analysis that will be further described, a scan in toroidal mode number will be performed assuming the frequency separation between the modes is caused by the Doppler shift due to toroidal rotation of the plasma.

The signals from Mirnov coils show in Fig.2 that a large amplitude n=2 neoclassical tearing mode (NTM) at frequency of ≈25 kHz was excited at ~ 8.4 s. This mode caused multiple high-frequency harmonics in the reflectometry and interferometry diagnostics, thus making the high frequency range of the perturbed density measurements polluted and the identification of possible α-particle driven AEs very difficult in the presence of NTM, i.e. after ~ 8.4 s. In order to avoid misinterpretation of the high frequency data, we only consider in our further analysis the high frequency modes in the TAE frequency range that were observed before the start time of the NTM (so we exclude these modes to be harmonics of the NTM).

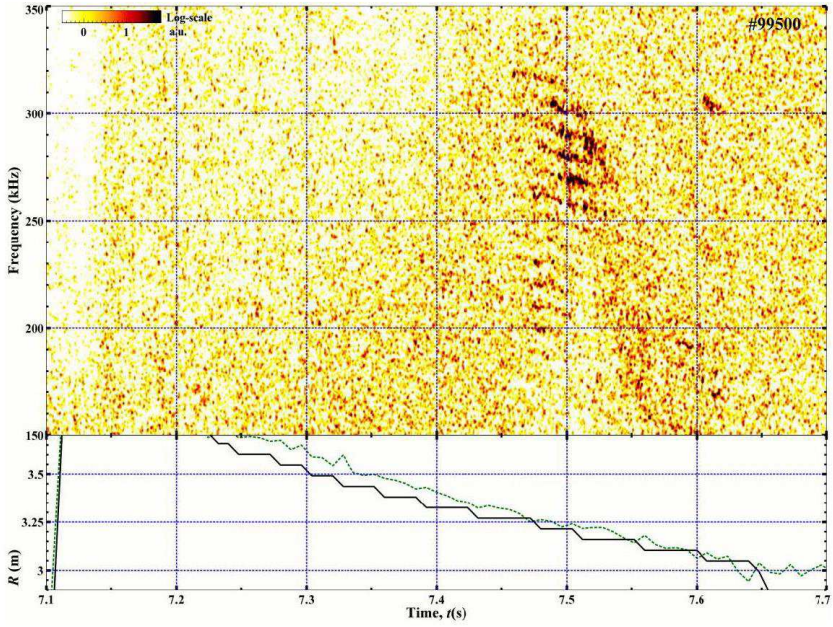

Figure 4. Top: Spectrogram of δn perturbations measured with a sweep-frequency reflectometer. Bottom: major radius of the reflectometer layer as a function of time.

3.1 Alpha-particle parameters from TRANSP modelling of discharge #99500

To assess the evolution of the plasma parameters and DT fusion products in a self-consistent way, the transport code TRANSP was used for the interpretative analysis of the discharges [20]. The temporal evolution of the electron density and temperature profiles used as input to TRANSP were measured with high-resolution Thomson scattering and multi-channel ECE shown in Figs.5, 6. Note that Fig.6 shows that T_e profile became hollow after ~ 9 s as a consequence of the non-mitigated tungsten accumulation and consequent increase in core plasma radiation up to ~ 4 MW as Fig.2 shows.

The measured total neutron rate with that computed by TRANSP are shown in Fig.7. One can see that the dominant fusion yield is determined by the beam-plasma reactions, with the thermonuclear fusion contributing about ~ 10% only and with beam-beam fusion noticeable only during the short slowing-down time between the switch from T-beams to D-beams. Fig.7 also shows the TRANSP over-prediction of the neutron rate by up to ~ 25% typical of JET discharges with beam-plasma dominant neutron yield [20] and relates to both phases of T-NBI and D-NBI heating. It is important to note that a high accuracy calibration of 14 MeV neutron emission has been performed just before the DTE2 campaign [21] and this was used in the measurements in Fig.7.

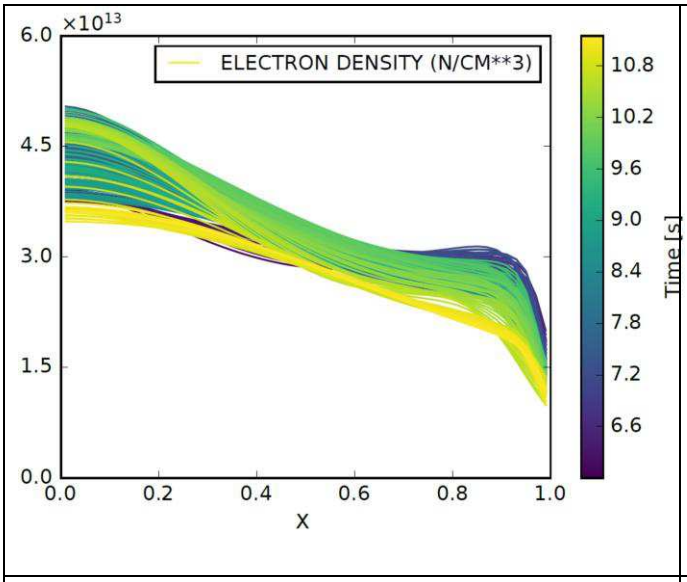

Figure 5. Profiles of electron density as functions of X= (R- R_0) /a for the color-coded time slices.

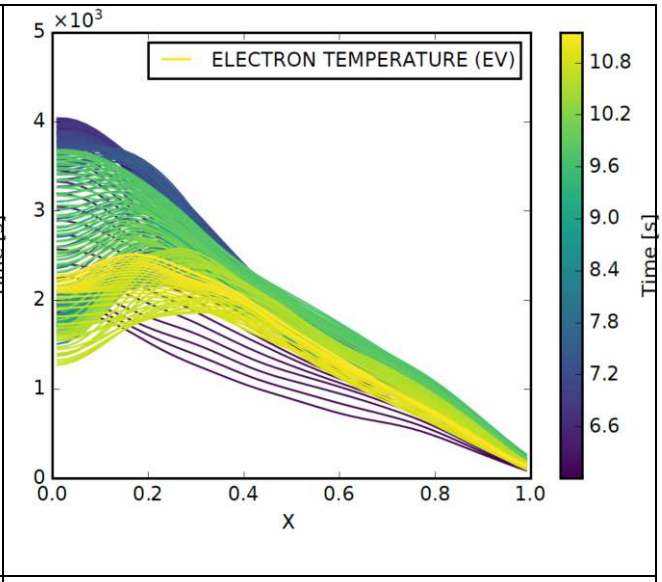

Figure 6. Profiles of electron temperature as functions of X= (R- R_0) /a for different color-coded time slices.

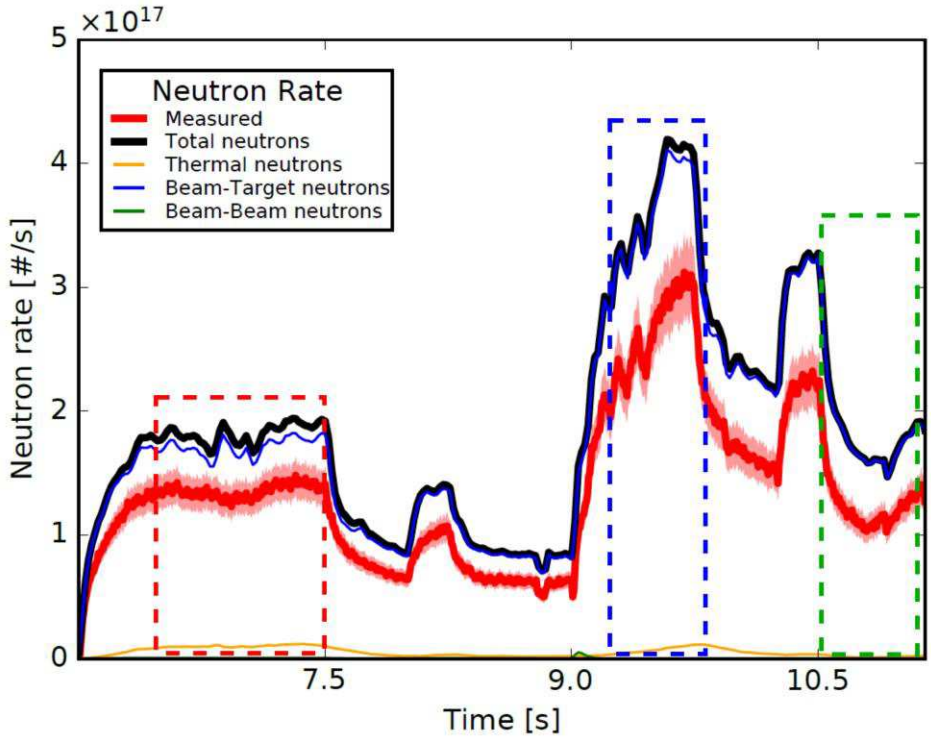

Figure 7. Temporal evolution of the measured (red) neutron rate versus TRANSP computed neutron rate (black) in JET discharge #99500. The time of the change of T-beams into D-beams is 9 s and the time intervals used in TRANSP analysis that will follow for assessing α-particles are: T-beam (red broken), the start of D-beam (blue), and the end of D-beam (green).

α-particle characteristic properties computed with the TRANSP code are shown in Figs.8-10. The radial profiles of the α-particle pressure shown in Fig.8 correspond to the time windows of T-beam (red) and D-beam (blue). These profiles are very peaked and have a very small population of α-particles outside the half-radius. On the other hand, the α-particle profile at the end of the discharge has a much lower value of $p_\alpha(0)$ and is weakly reversed due to the hollow T_e -profile shown in Fig.6.

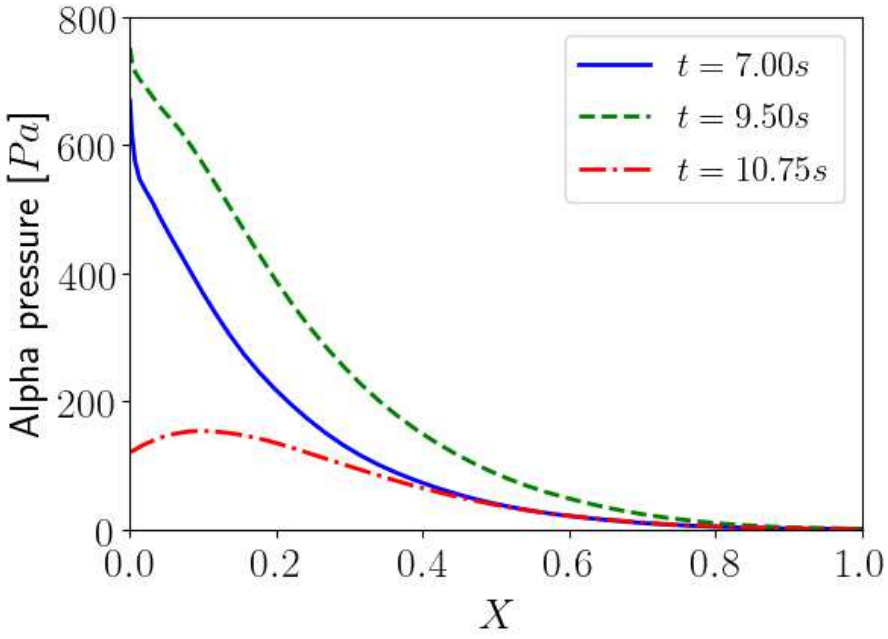

Figure 8. Profiles of α-particle pressure as functions of X= (R-R_0) /a averaged in time over the time windows shown in similar colours in Fig.7.

igures 10, 11 show the temporal evolution of α-particle energy averaged over the distribution function and slowing-down time computed with the TRANSP code. It is seen in Fig.10 that the α-particle averaged energy is in the range of ~ 3 – 3.2 MeV at the beginning of the discharge, but decreases eventually down to ~ 1 MeV roughly corresponding to the kinetic temperature of the α-particle slowing-down distribution. Figure 11 shows that the slowing-down time of α-particles has its maximum value of ~ 0.35 s at the beginning of the discharge, but decreases down to half of this value at the end of the pulse.

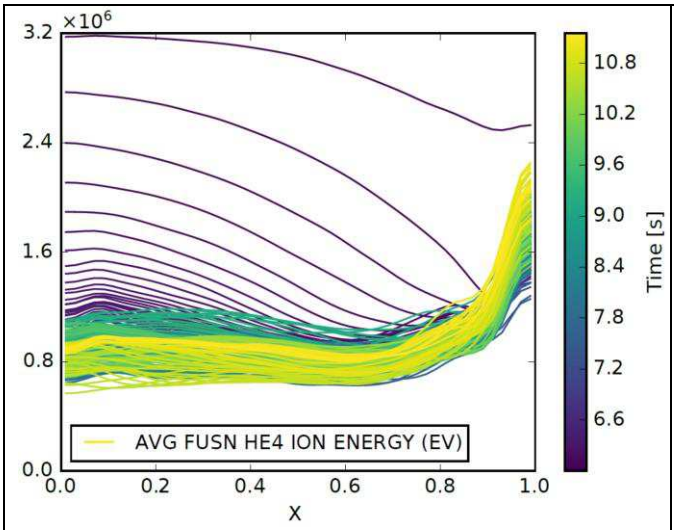

Figure 9. TRANSP modelling of temporal evolution of the profiles of α-particle energy averaged over the distribution as functions of X= (R-R_0) /a in JET discharge #99500.

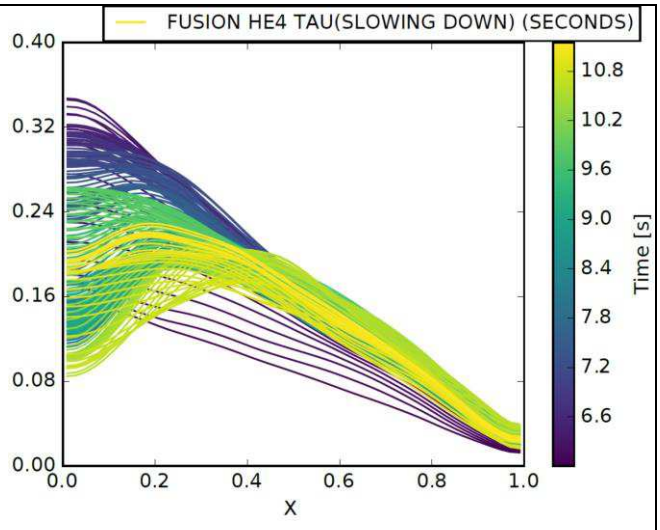

Figure 10. Time evolution of α-particle slowing-down time profile as functions of X= (R-R_0) /a in JET discharge #99500.

3.2 Interpretation of the high-frequency modes observed in JET discharge #99500

In the discharge considered, the high-frequency modes shown in Fig.4 appear at ~ 180 kHz – 325 kHz as the T-beam power drops from 9.4 MW to 6.0 MW. The modes are not seen in the Mirnov coils, most likely due to their core localisations and low amplitudes, and so the toroidal mode numbers could not be determined. The modes are localised at major radii ~ 3.15 m – 3.25 m corresponding to r/a ~ 0.15 – 0.25, and they are best seen at 7.5 s.

Modelling with the HELENA [22], CSCAS [23], and MISHKA [24] codes was performed in order to identify the modes observed at 7.5 s. First, the equilibrium was reconstructed with the EFTM code constrained by the motional Stark effect and with the MHD marker from the reflectometry showing the position of the magnetic flux surface corresponding to q=3/2 near R=3.3 m at t = 8.2 s – 10.6 s. Ion density profiles were taken from an interpretative TRANSP run. Figures 11 and 12 show the safety factor and ion density profiles correspondingly.

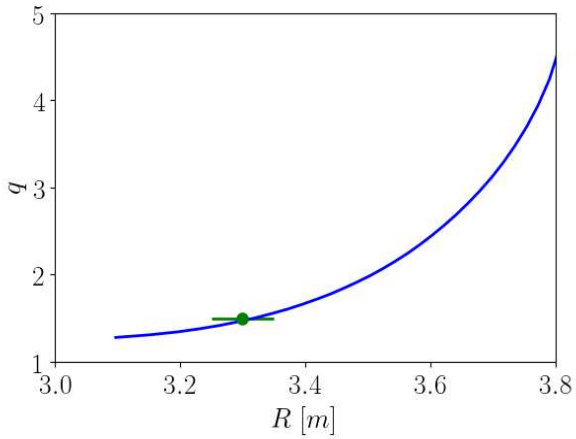

Figure 11. Profile of the safety factor $q(R)$ used in the MHD modelling of #99500, t= 7.5 s. The MHD marker is indicated by the green dot with error bars.

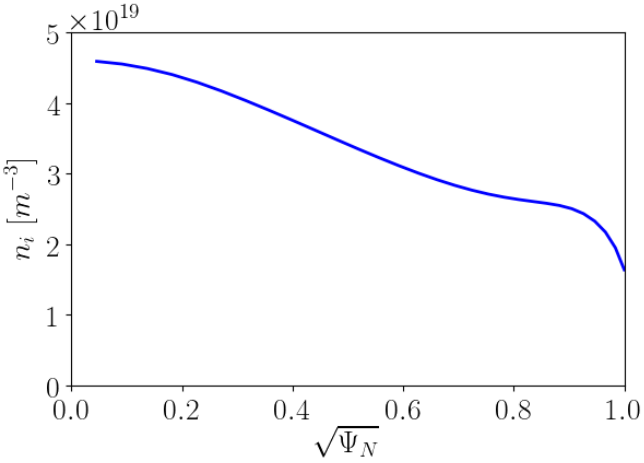

Figure 12. Profile of the mass ion density computed with the TRANSP code for #99500, t=7.5 s. Here, the square root of the normalised toroidal flux is $\approx r/a$ where a =1 m is the minor radius.

Scans in the toroidal mode numbers and the mode frequencies were performed and ~ 100 TAEs were computed for the reconstructed equilibrium with the MISHKA code. By taking into account the core localisation of the experimentally observed modes, only TAEs localised within $r/a \approx 0.25$ were selected for the best fit between modelling and observations.

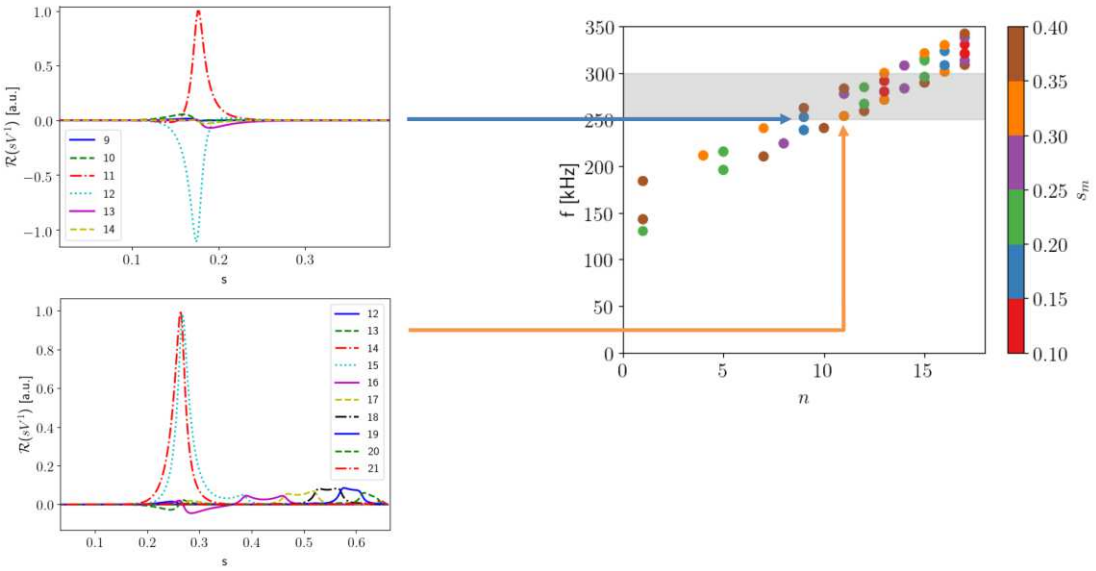

Figure 13. Left: Odd (i.e. sign (V_m)= - sign(V_{m+1})) (Top) and even (sign (V_m)= + sign(V_{m+1})) (bottom) core-localised TAEs with n = 9 that fit the radial localisation among all TAEs with the relevant computed frequencies (right).

It was found that TAEs with toroidal mode numbers in the range $9 \leq n \leq 16$ are in the right radial location and frequency range for interpreting the modes observed. Figure 13 shows two examples of the TAE mode structures computed with the MISHKA code.

4 Beam modulation discharges in JET DT plasma

Following the test discharge #99500, three discharges were performed (pulses ##99501, 99503, and 99627) with injection of D-beams into T-rich plasmas. Different maximum power levels of the NBIs were employed in these discharges, P_{NBI}= 10 MW in #99501, P_{NBI}= 11.5 MW in #99503, and P_{NBI}= 14.5 MW in #99627, and somewhat different D:T concentrations were used, D:T≈ 33:67 in #99501, D:T≈ 35:65 in #99503, and D:T≈ 40:60 in #99627. The maximum neutron rates achieved $R_{NT} \approx 3.7\text{x}10^{17}$ s^{-1} in pulse #99501, $R_{NT} \approx 4.45\text{x}10^{17}$ s^{-1} in pulse #99503, and $R_{NT} \approx 5.7\text{x}10^{17}$ s^{-1} in pulse #99627. The temporal evolution of the neutron rate and of the D-beam power in these three discharges are shown in Figure 14.

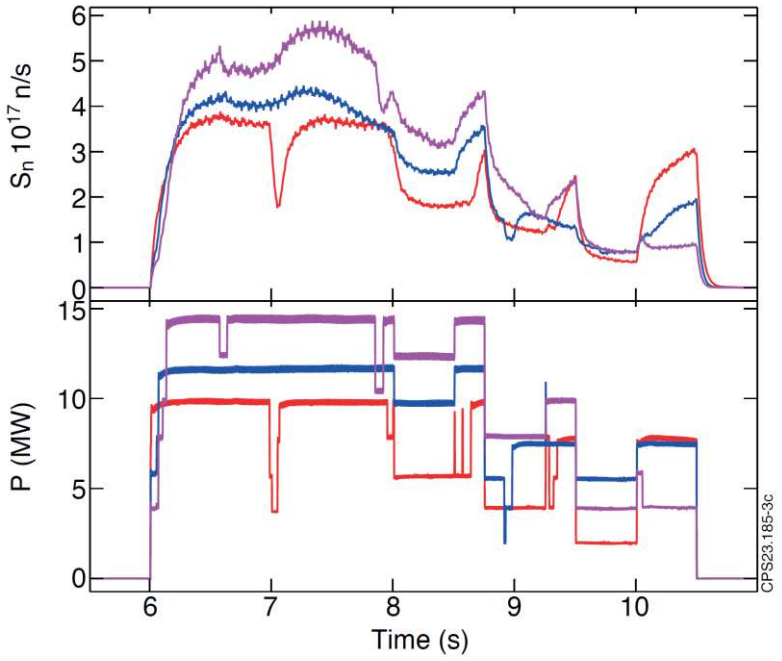

Figure 14. Top: DT neutron rates in discharges #99501 (pink), #99503 (red), and #99627 (blue). Bottom: the corresponding waveforms of the modulated NBI power.

Two comparison discharges with injection of T-beam into D-rich plasma and with injection of D-beam into D-plasma were also performed. The discharge with T-beam injection into D-rich plasma (JET pulse#99502) was aimed at providing a different NBI damping effect on possible AEs excited, while the D-only discharge (JET pulse #100797) provided the information on possible pollution of the AE frequency spectrum due to the diagnostic specific features. The objective of comparing these discharges is avoiding an incorrect identification of α-particle driven AEs in DT plasmas. JET discharge #99502 with T-beam injection had a maximum power of NBI P_{NBI}= 13 MW and D-rich mixture of D:T≈ 55:45; it achieved maximum neutron rate $R_{NT} \approx 3.3\text{x}10^{17}$ s^{-1} as Figure 15 shows. The discharge with pure D plasma and D-beam injection had a maximum power of NBI P_{NBI}= 12 MW and NBI power waveform and plasma parameters closely matching those of the DT discharges as Figure 16 shows.

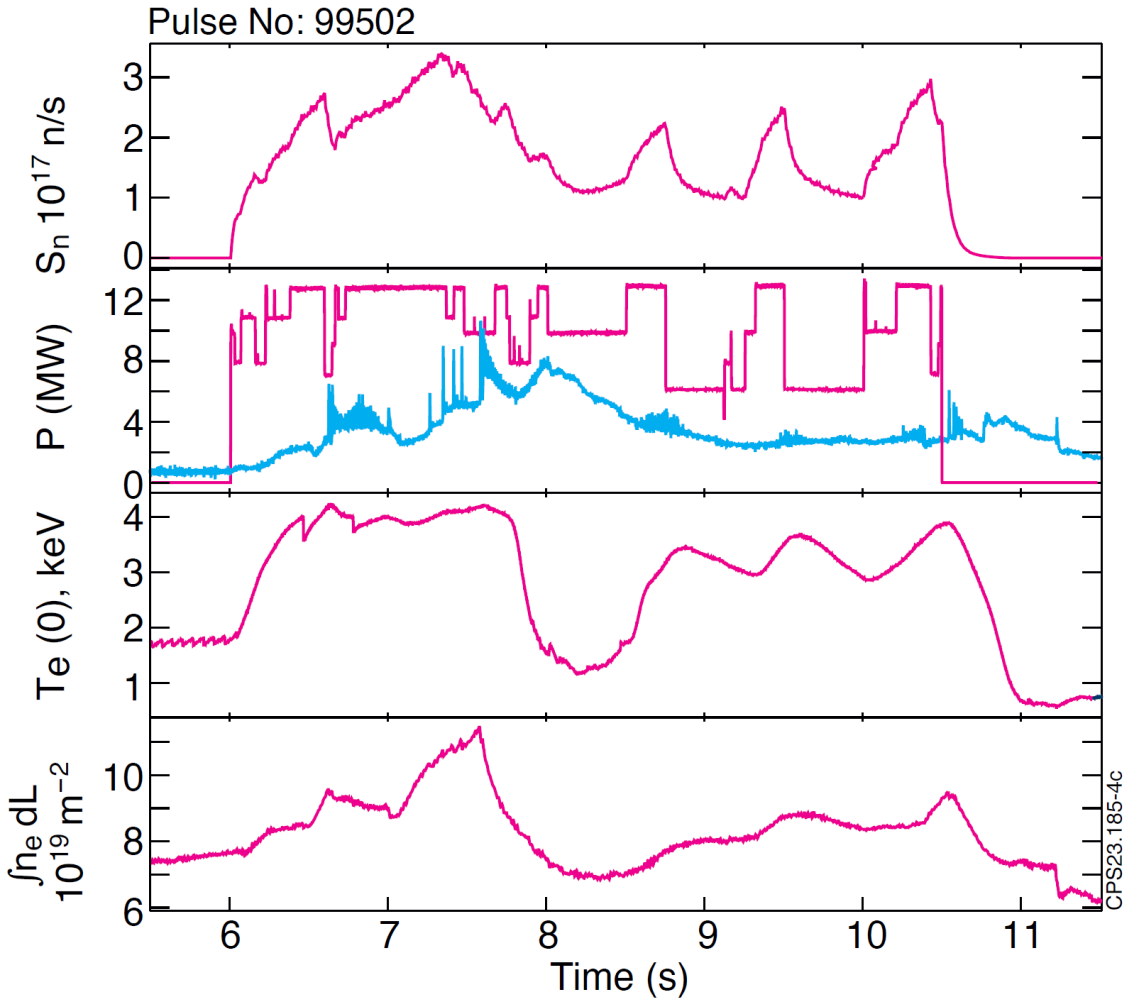

Fig.15 From top to bottom: DT neutron rate in discharge #99502 with D:T≈ 55:45; waveform of T-beam power and the power of plasma radiation; on-axis electron temperature from ECE measurements; line-integrated electron density measured with high time resolution by interferometry.

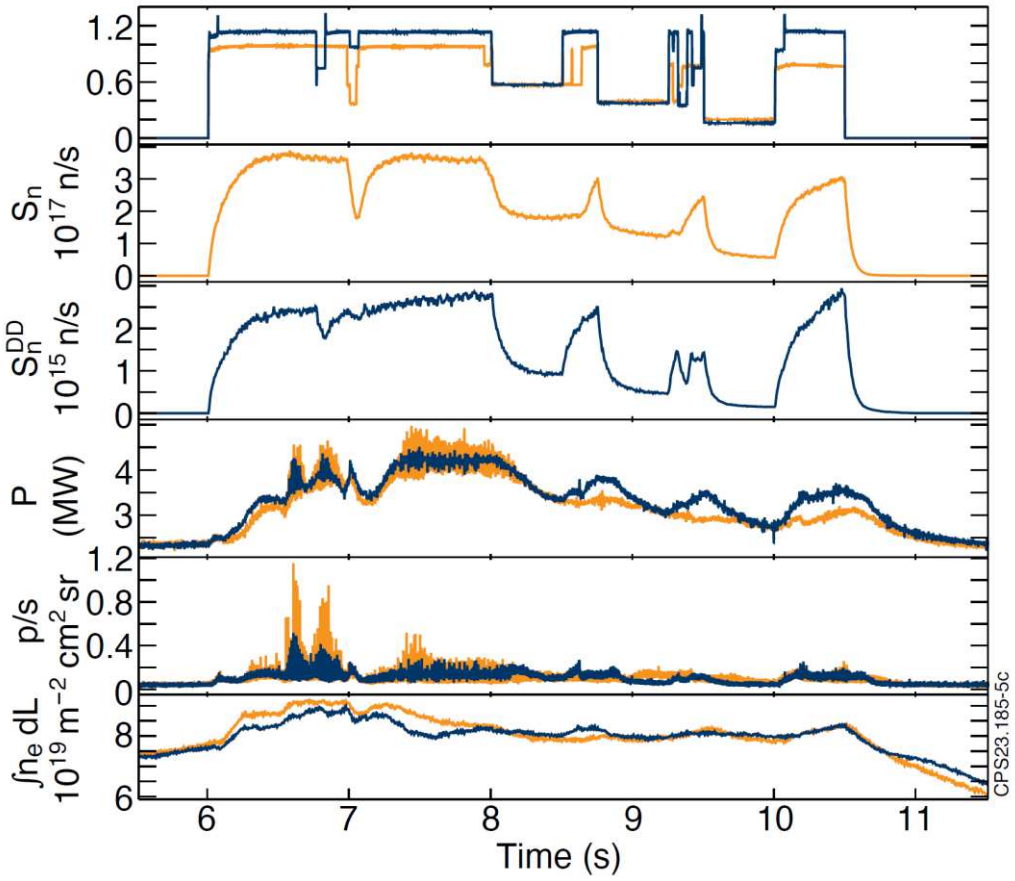

Fig.16 From top to bottom: NBI power waveforms in DT discharge #99501 (gold) versus the comparison D-only discharge #100797 (blue); temporal evolution of DT neutron rate in #99501; temporal evolution of DD neutron rate in #100797; comparison of plasma radiation power in #99501 and #100797; comparison of ELM activity in #99501 and #100797; comparison of line-integrated electron density measured with high time resolution by interferometry in #99501 and #100797.

4.1 Alpha-particle distribution achieved in DT discharges with NBI modulation

Measurements of lost α-particles were performed with the SP in all DT discharges and in all of them a double-hump in the pitch-angle was observed in the lost α-particle distribution similar to the discharge #99500. Figure 17 shows an example of the SP measurements.

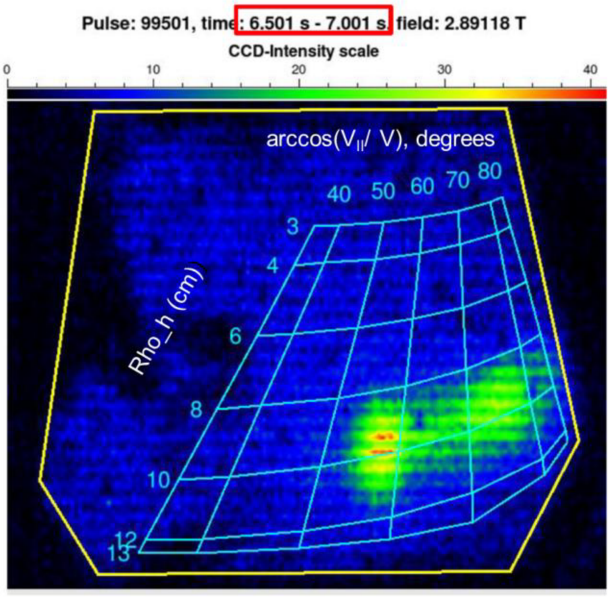

Figure 17. Data from scintillator plate showing counts of lost α-particles with Larmor radii in the range ~8–11 cm and pitch-angles in the range ~55° – 80° over the time interval 6.5 – 7.0 s.

For assessing the possibility of a bump-on-tail in the α-particle distributions in the DT discharges, the FIDIT code [14] was used in 1D approach first for a particular case of the pitch angle of counter-current passing α-particles similar to the one used in [12]. The following Fokker-Planck equation was investigated with the source of α-particles modulated by the beam:

$$\frac{\partial F}{\partial t} + \frac{1}{v^2}\frac{\partial}{\partial v}\frac{v^3 + {v_c}^3}{t_s}F = S\left(v, \frac{v_\parallel}{v}, t\right),$$

$$S\left(v, \frac{v_\parallel}{v}, t\right) = S_{target-target}(v) + S_{beam-target}\left(v, \frac{v_\parallel}{v}, t\right),$$

where F is the distribution function of α-particles, v_c is the critical velocity corresponding to the equal flows of energy from α -particles to thermal electrons and ions, $v_\parallel$ is the component of the α -particle velocity parallel to the magnetic field, and S is the intensity of the α-particle source consisting of two dominant components, the beam-plasma (beam-target) and the thermonuclear (target-target) α-particles. The characteristic slowing-down time of energetic ions is mostly determined by the collisions with plasma electrons as:

$$t_s = 6.3 \cdot 10^{14} \frac{A_H T_e^{3/2}}{Z_H^2 n_e ln\Lambda_e},$$

where A_H, Z_H are the mass (in hydrogen mass units) and the charge number of the energetic ions, n_e(m^{-3}) is the electron density and $ln\Lambda_e \approx 16$ is the Coulomb logarithm.

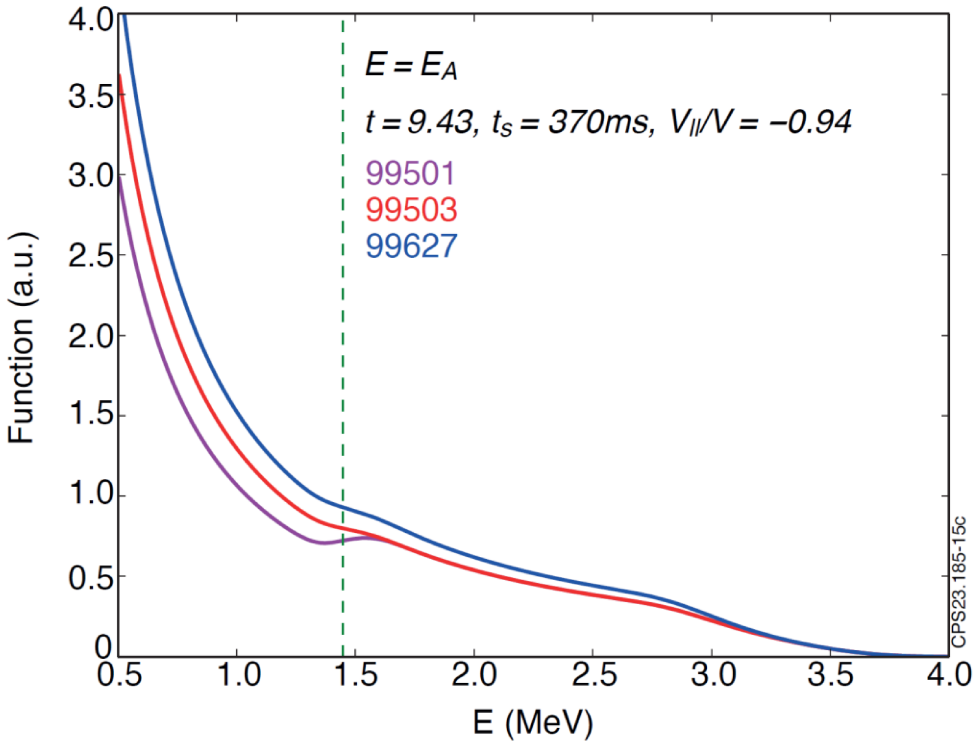

Figure 18. The FIDIT results: computed α-particle energy distributions for a particular pitch-angle value of $\frac{v_\parallel}{v}$ = -0.94 [12] for plasma parameters in the three comparison discharges shown in Fig.15.

The results of the FIDIT computations are shown in Fig.18 for a particular pitch-angle of the α-particles. It is seen that although all three distribution functions in the comparison discharges deviate notably from the slowing-down distribution, but only one of them in discharge #99501 has a bump-on-tail at the position of the Alfvén resonance $E = E_A$ at the time chosen.

TRANSP was then used to assess the α-particle distribution function. First, the time interval with the most significant deviation from the slowing-down distribution was identified. This corresponded to the final NBI modulation phase of highest amplitude, from 10.0 s onwards in discharge #99501 as Fig.19 shows. To detect the bump-on-tail features in the fast ion distribution, TRANSP runs used a fine time resolution of 5 ms in the interval between 10.0 s and 10.09 s, with the number of the markers set to 5x10^5. Figure 20 shows the resulting distribution functions computed for the different time intervals, with positive gradients of the distributions in energy found to exist over a wide range

of energies at different times as Fig.21 demonstrates. It is important to note the dynamic evolution of the BOT on a quite short time scale, which displays a transient character of the BOT at any given resonant energy. These BOT calculations with the TRANSP code broadly agree with the simplified FIDIT results described above.

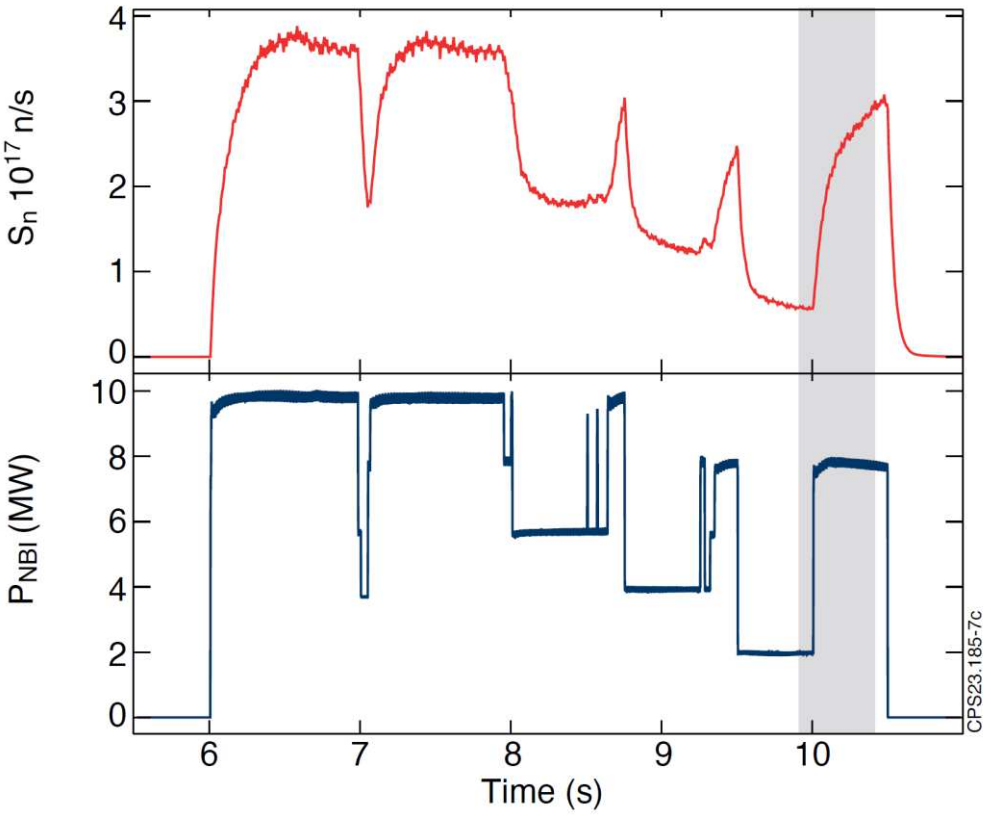

Figure 19. The neutron rate (top) and modulated NBI power wave-form (bottom) in JET discharge #99501. The grey shaded time interval shows the TRANSP modelling of α-particle distribution function.

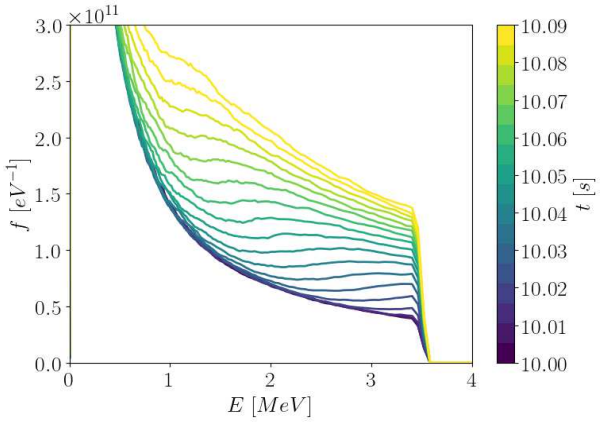

Figure 20. The computed α-particle distribution functions in the time interval from 10.0 s to 10.09 s with step of 5 ms.

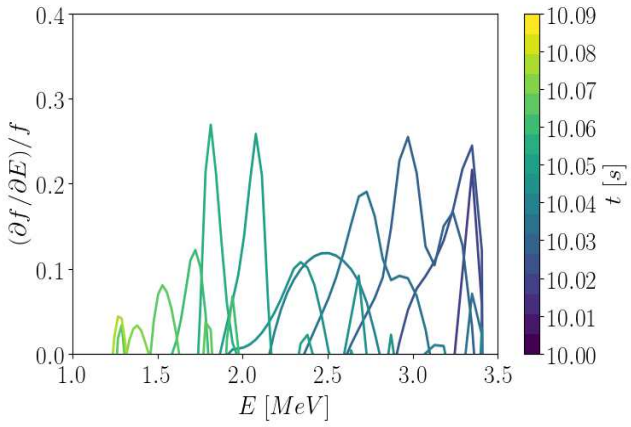

Figure 21. The energy derivatives of the computed distributions where they are positive corresponding to a BOT.

4.2 High-frequency modes observed in dedicated DTE2 discharges with modulated NBI on JET

Three main types of high-frequency modes were detected in the BOT DTE2 pulses, apart from the obvious harmonics of low-frequency MHD modes:

i) Before the NBI modulation, some modes are detected in the TAE frequency range. These are detected with the sweeping-frequency reflectometry, interferometry, and SXR. The modes were observed in #99503 and are described in detail in [25];

ii) Stand-alone "smooth frequency" single modes very highly localised at the magnetic axis with frequencies below the TAE frequency range. These are seen by the interferometry looking through the plasma centre and in the on-axis SXR channels;

iii) Numerous pulsating amplitude high-frequency modes are seen in a very wide frequency range up to ~ 450 kHz. These start just before NBI power modulation and last up to ~ 0.6 s (e.g. in JET DT pulse #99627). These modes are seen in the interferometry and SXR channels looking through the plasma centre, within radius up to r/a ~0.25.

We now consider each of the mode types and present their possible interpretation.

The modes of type (i) are considered in detail in [25] for JET discharge #99503 in which the most complete set of plasma diagnostics was available. The conclusion [25] is that case (i) of the modes

observed corresponds to core-localised TAEs with rather high toroidal mode numbers which are affected strongly by the beam drive and the radiative damping, but the small α-particle drive still plays a decisive role to excite the mode at the very threshold caused by the balanced drive and damping. The modes of type (i) were observed before the intended modulation of the α-particle source and hence no BOT effects contribute to the α-particle drive estimate, only the radial gradient of α-particle pressure provides the drive.

To analyse the modes of type (ii) we consider JET discharge #99501 with DT plasma and the similar discharge #100797 performed with D beam injected into pure D plasma. Figure 22 displays the mode of interest observed in DT discharge #99501 in the frequency range of ~70 -90 kHz during the time interval from ~7.1 s to ~7.13 s. Although the mode frequency is below the expected TAE frequency range, the mode is definitely not associated with harmonics of any low-frequency MHD, and it is seen simultaneously in the interferometry and SXR just after a short-period notch in the NBI power performed for diagnostic purposes. The drive from NBI-produced energetic ions could be the most likely source of this mode excitation but this does not involve α-particles and will be studied elsewhere. Also, the continuous modes seen at $\approx$ 5 – 15 kHz in the interferometry signal are interpreted as NTMs driven by thermal plasma pressure and not associated with α-particles.

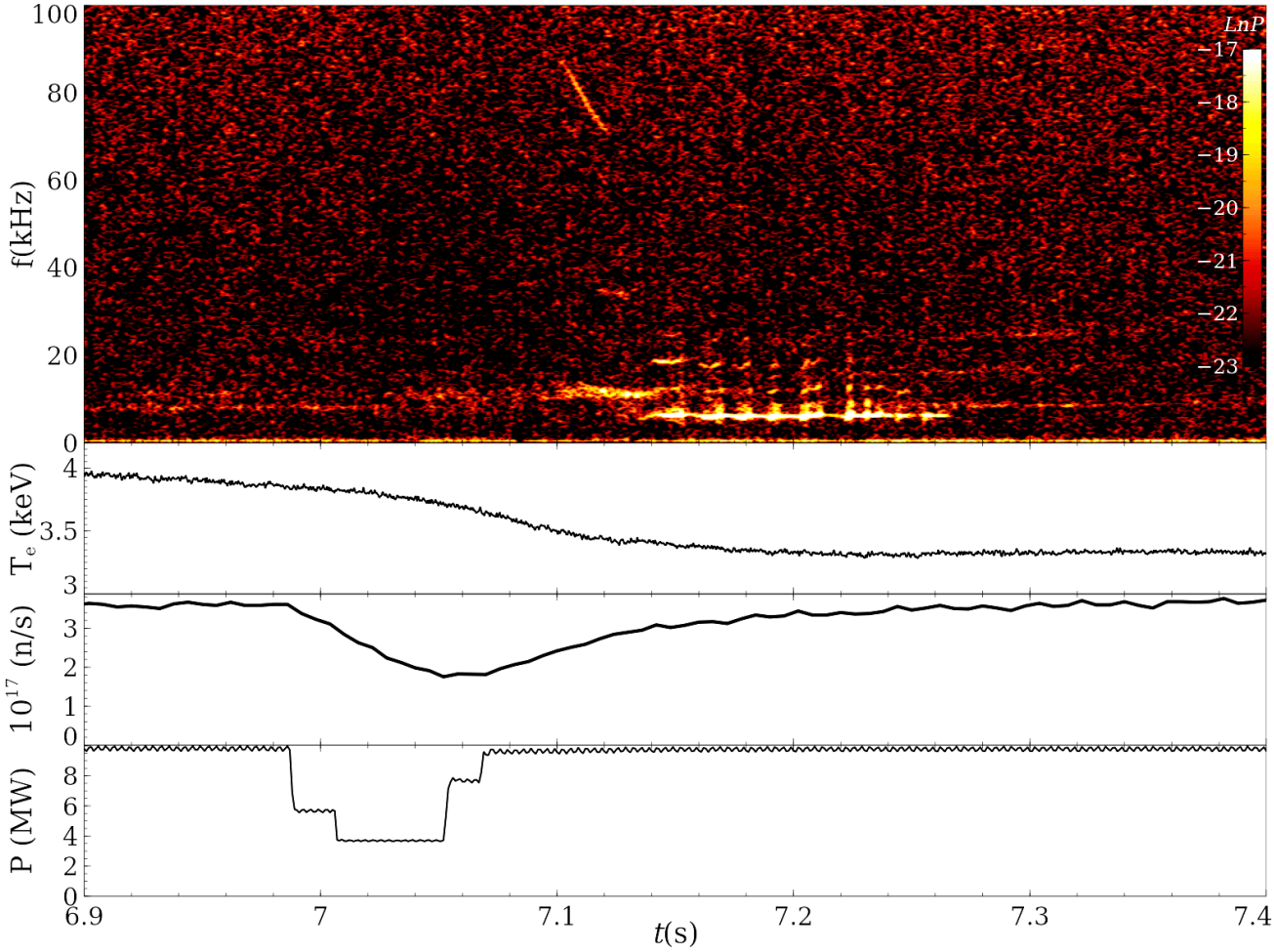

Figure 22. From top to bottom: spectrogram of δ*n* perturbations measured with interferometer with vertical line-of-sight through the magnetic axis in DT discharge #99501; on-axis electron temperature measured with ECE; temporal evolution of the DT neutron rate; temporal evolution of D-NBI power.

Although the mode observed in Fig.22 looks like a possible candidate for α-particle driven modes, an observation of a similar mode in pure D discharge with D beam excludes this interpretation. Figure 23 shows the spectrogram for D-only discharge #100797 where a perturbation is seen in the similar frequency range of ~ 80 kHz at a similar time from ~7.23 s as in the DT discharge #99501. Due to the similarity of the modes (ii) in DT and D plasmas, these were discarded as possible genuine modes excited by α-particles.

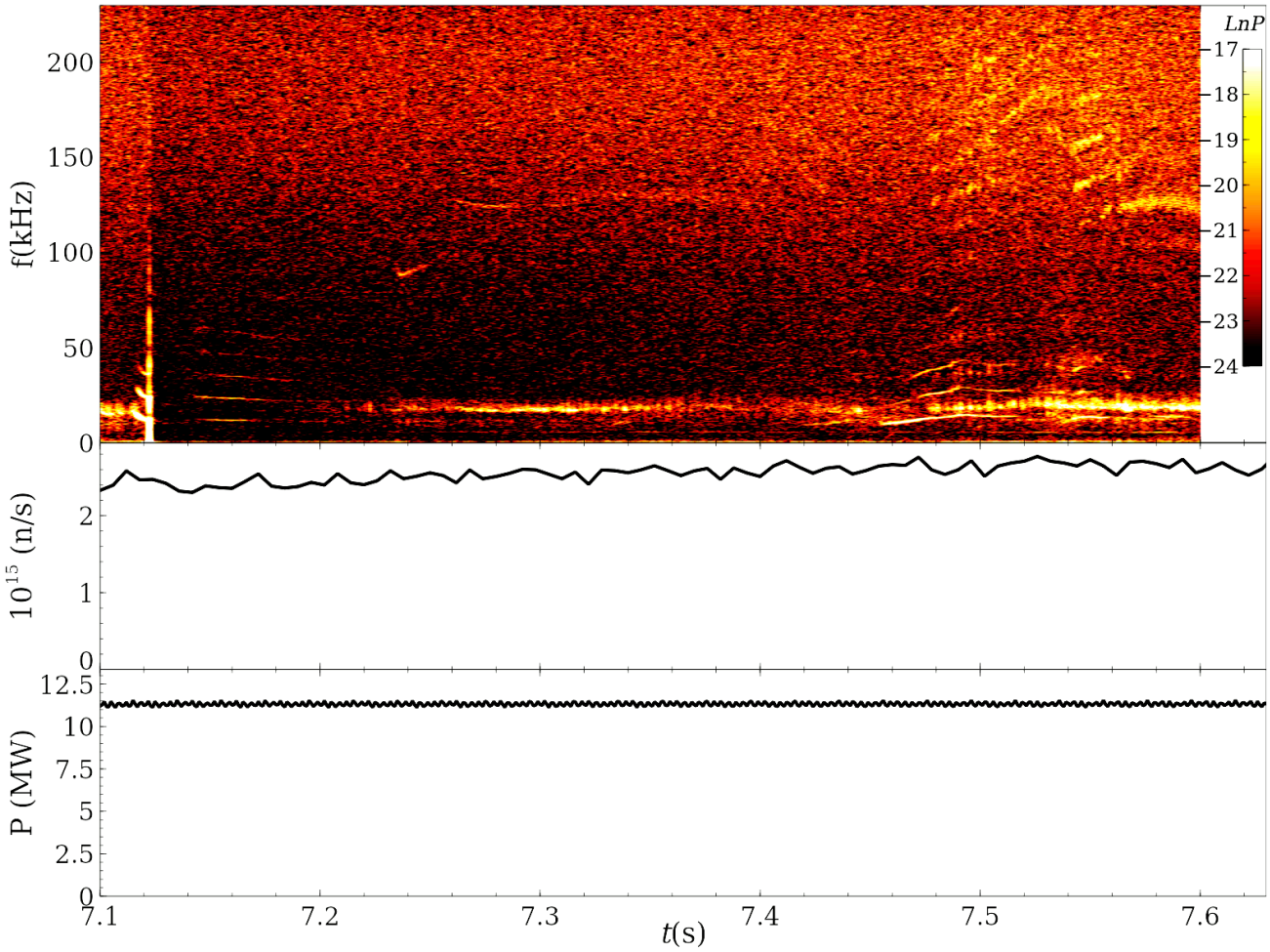

Figure 23. From top to bottom: spectrogram of perturbations measured with SXR Channel 10 looking through the magnetic axis in D discharge #100797; temporal evolution of the DT neutron rate; temporal evolution of NBI power.

In case (iii), multiple short-living modes in a wide frequency range up to ~ 450 kHz have been detected with interferometry, SXR camera and reflectometry as Figure 24 shows. The modes observed were localised close to the magnetic axis as can be seen from Figure 25 where the spectrogram of SXR Channel 10 shows the modes at the magnetic axis. However, the modes become of lower amplitude in Channels 9 and 11, and no modes are seen in Channel 12 at about r/a ~ 0.25. Figure 26 shows a zoom of the modes from Fig.25 so their pulsating character is clearly visible. These modes were not seen in Mirnov coils thus making their toroidal mode numbers n's undetermined. No similar activity has been detected in discharge #100797 with pure D plasma.

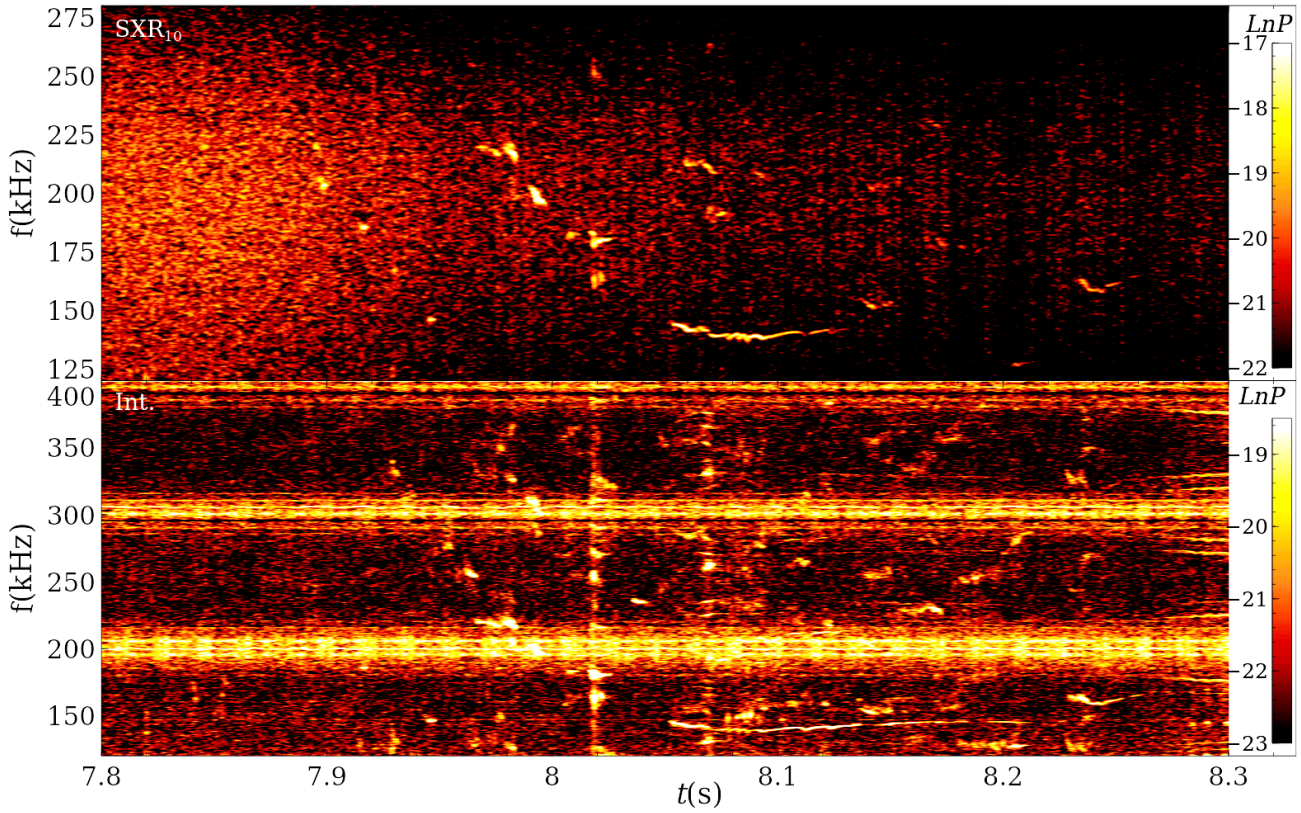

Figure 24. Top: the pulsating amplitude modes going down in frequency with time in #99502 seen in the SXR Channel_10 (through the magnetic axis). Bottom: same modes seen with interferometry vertical line-of-sight near the magnetic axis.

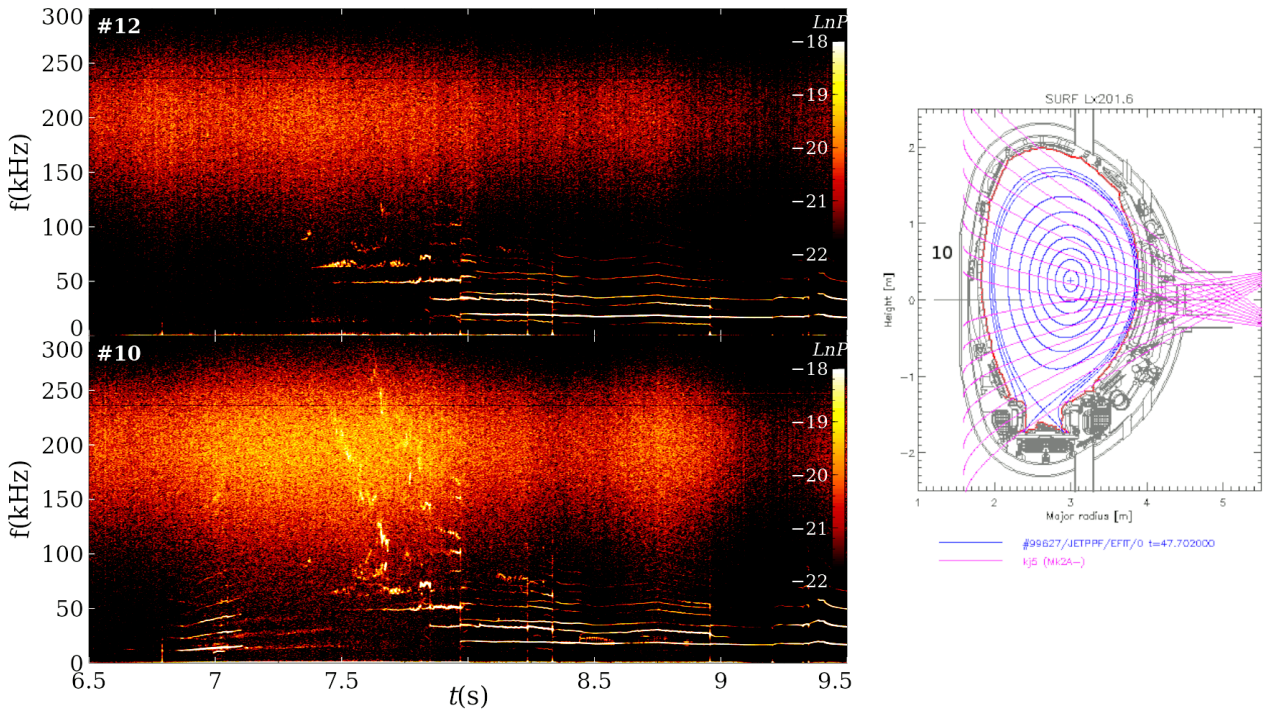

Figure 25. Bottom left: the pulsating amplitude modes in frequency range 100-300 kHz seen with SXR camera Channel 10 in D-T pulse #99627. Top left: no similar modes are seen with SXR camera Channel 12 in the same discharge. Right: geometry of the SXR camera with the Channel 10 indicated.

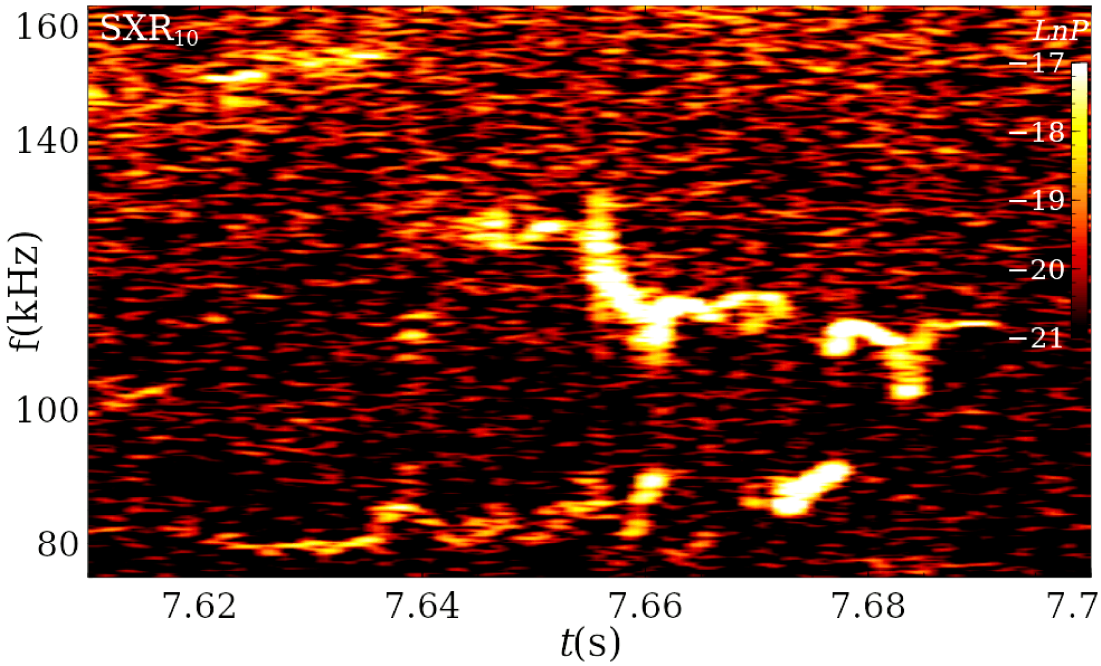

Figure 26. Zoom of Fig.25 showing the pulsating amplitude modes seen with SXR camera Channel 10 in D-T pulse #99627.

Interpretation of these modes could be given in terms of the on-axis kinetic Alfvén eigenmodes described by Rosenbluth and Rutherford in [1], let us call these "RR modes". These on-axis modes are eigenmodes of kinetic Alfvén waves (KAW) having their reflection points surrounding the magnetic axis. The dispersion relation of KAW with the first order finite Larmor radius (FLR) effect of thermal ions has the form [1, 4]:

$$\omega^2 = k_{\|}^2 V_A^2 (1 + k_{\perp}^2 \rho_i^2 \left(\frac{3}{4} + \frac{T_e}{T_i}\right)). \qquad (1)$$

In contrast to shear Alfvén wave, KAW can propagate across the magnetic field, and it has the electric field components not only across the magnetic field, but also in the direction of the magnetic field. Equation (1) shows that if a KAW propagates through a region with $k_{\|} = 0$, i.e. across a rational magnetic surface in a tokamak, it becomes of an infinitely short wave-length, $k_{\perp} \to \infty$, as its frequency is constant. In such case, the first order FLR becomes inadequate for describing the wave, and full order FLR is required for the wave description. However, the case of RR modes does not

have $k_{\|} = 0$ between the KAW reflection points surrounding the magnetic axis, and the first order FLR is sufficient for the eigenmode description.

The KAWs have their frequency above the shear Alfvén continuum as the sign "+" in Eq.(1) shows, and so a "potential well" formed by the radial structure of the Alfvén continuum is needed for two reflection points of KAW to exist surrounding the magnetic axis and forming an RR eigenmode between them. Since the original paper [1] was written before the role of the poloidal harmonic coupling became well-known due to toroidicity, ellipticity, and triangularity, only single poloidal harmonic was involved in the structure of RR modes of [1]. For real tokamak geometry, however, several frequency ranges emerge at the TAE-frequency, EAE-frequency, and NAE-frequency, where on-axis potential wells could emerge as $q(r=0, t)$ decreases in time and the dominant poloidal harmonics at the magnetic axis sweep. This results in the possibility of the RR modes to occur transiently over a broad frequency range as $q(0)$ evolves.

For computing the RR modes we incorporate the first order FLR effects in the form of complex resistivity [26] with dominant imaginary part (representing the non-dissipative FLR effect) in the MISHKA code [24]. Figure 27 shows typical on-axis RR-modes with n=5 and normalised frequency $\lambda=\omega R_0/ V_A(0)$ computed in such approach for the on-axis safety factor $q(0)$ = 1.22 in JET discharge #99502.

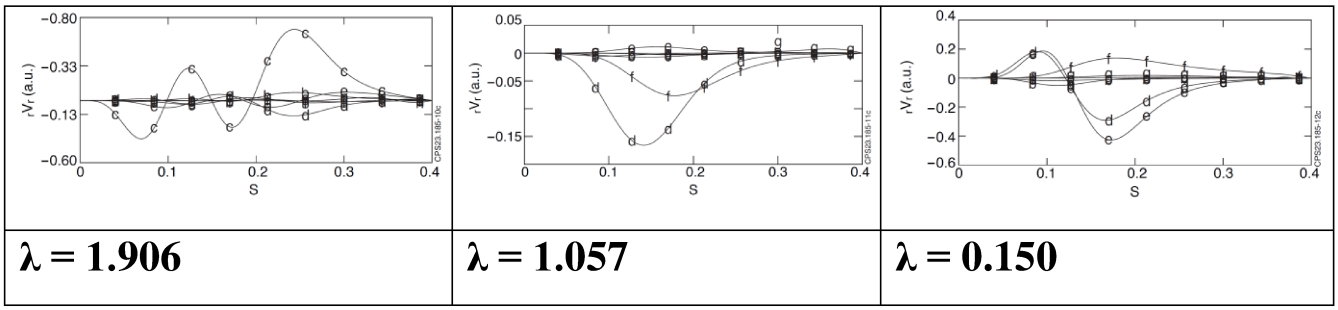

Figure 27. The wave potential variable $s*V^1 \approx rV^r$ as a function of $s=(\psi_P/ \psi_P(a))^{1/2} \approx r/a$ for the n = 5 Rosenbluth-Rutherford modes [1] computed for $q(0)$=1.22. The normalised frequency is given by $\lambda=\omega R_0/ V_A(0)$, and the poloidal harmonics labelled c, d, e, f correspond to m= 9, 8, 7, 6.

One can see that the modes found mostly consist of a single poloidal harmonic though some other harmonics may be present depending on the proximity of the RR eigenfrequency to the relevant frequency gaps determined by toroidicity, ellipticity, or triangularity. Although the physics of the modes shown in Fig.27 correspond to the same KAW with first order FLR description, the modes appear in significantly different frequency ranges, from the highest frequency NAE to more than ten

times lower sub-TAE frequency. The radial structure of the RR modes depends on the proximity of the mode frequency to the bottom of the "potential well" near the magnetic axis, and it can have radial mode numbers from the lowest values of l=0 and l=1 (boxes two and three in Fig.27) to rather high ones similar to those shown in [1] (first box in Fig.27). Taking into account the transient character of the potential wells and potential hills formed at the magnetic axis as $q(0)$ decreases, and the energetic particle drive modulated on purpose, the appearance and excitation of the RR modes would look as numerous on-axis modes excited transiently over broad frequency range nearly randomly.

Figures 28, 29 illustrate the high sensitivity of the continuum spectrum to the value of $q(0)$. While the Alfvén continuum structure at $q(0) = 1.22$ in Fig.28 forms three potential wells on-axis and can support RR-modes in these potential wells at three different frequencies, the Alfvén continuum at slightly different value of $q(0)$=1.16 shown in Fig.29 loses these three potential wells and no RR-modes on-axis are found associated with the "new" wells. This sensitivity can explain the intermittent character of the on-axis modes observed in JET DTE2 experiments.

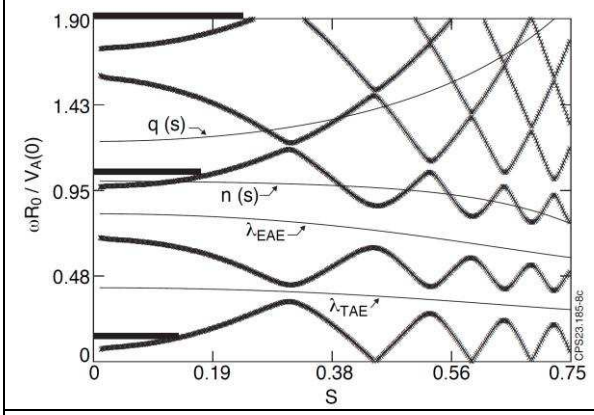

Figure 28. Alfvén continuum structure for $q(0)$=1.22. RR-modes marked with three horizontal thick lines exist in the 3 potential "wells" on-axis. Here, $\lambda_{TAE} = \omega_{TAE} R_0 / V_A(0)$ and $\lambda_{EAE} = \omega_{EAE} R_0 / V_A(0)$ are the normalised frequencies of the TAE- and EAE- centres of the relevant TAE and EAE gaps.

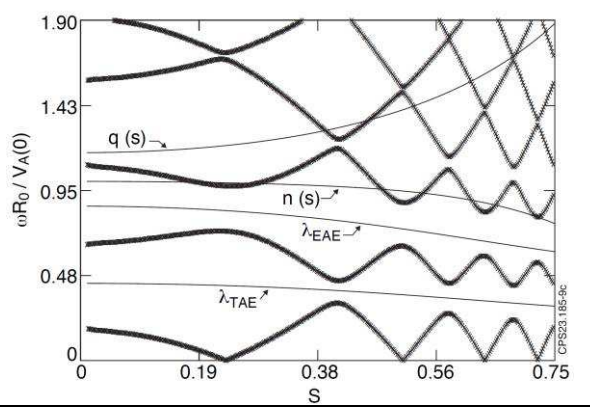

Figure 29. Alfvén continuum structure for the same equilibrium as shown in Fig.28, but for $q(0)$=1.16. No RR-modes found in this case.

This intermittent type of the mode existence looks similar to the type (iii) of the modes experimentally observed in the DT discharges described above. Since similar modes were not observed in the D-only comparison discharge, one concludes that these modes are excited by the fusion-born α-particles. The on-axis localisation of the modes suggests that the free energy source of the instability is a bump-on-tail in the α-particle distribution, $dF_\alpha / dE > 0$, rather than radial gradient of the distribution function. A complete investigation of the drive and damping of such modes remains however the subject of further studies as the highly non-standard near axis fast particle orbits and bump-on-tail effects go beyond the usual analyses of AE stability. Together with the unambiguous TAE excitation observed in the afterglow scenario of JET DTE2 discharges [13], the observation of the on-axis RR modes constitutes a wider picture of events to be observed in burning plasmas and shows the need in continuation of dedicated α-particle studies.

5. Summary

In summary, a scenario has been developed in JET with Be/W wall using NBI power modulation to achieve a bump-on-tail α-particle distribution in JET DTE2 discharges, and the transport analyses confirm the successful BOT formation. The analysis with the TRANSP code identified the main properties of α-particles and provided the basis, together with the equilibrium reconstruction techniques, for further studies of the α-particle effects on instabilities. Among three different types of high-frequency modes possibly excited by fusion-born α-particles and detected with reflectometry, interferometry, and SXR, i.e.

i) Modes detected in the TAE frequency range before NBI power modulation;

ii) Stand-alone "smooth frequency" single modes very highly localised at the magnetic axis with frequencies below the TAE frequency range;

iii) Numerous on-axis pulsating amplitude high-frequency modes seen in a very wide frequency range up to ~ 450 kHz.

the first type (i) was identified as high-*n* TAEs [25], the second type (ii) was discarded from the α-particle drive point of view as similar perturbations were observed in pure D reference discharge, and the third type (iii) of the modes was identified as the on-axis KAW eigenmodes predicted by Rosenbluth and Rutherford [1]. The calculations of all the drive and damping effects in the case of TAEs [25] have shown an important role of the beam ions in the mode drive, and the radiative damping – in the mode damping. Accurate consideration of all the smaller effects has revealed the importance of the α-particle drive that being small is likely to play nevertheless an important role in

TAE excitation at the very threshold of TAE instability determined by the balance of stronger damping and beam drive of the TAE observed. The significant activity of short-lived near-axis modes observed over wide frequency range is interpreted in terms of transient RR-modes evolving in time with the evolution of the on-axis safety factor $q(0)$. Although such modes were detected in the DT only discharges and hence these were likely to be driven by fusion-born α-particles, the issue of the α-particle drive for such on-axis modes is yet to be investigated. All these unique observations during JET DTE2 allow to validate and improve the codes used for predicting ITER and fusion power plants.

Acknowledgments

This work has been carried out within the framework of the EUROfusion Consortium, funded by the European Union via the Euratom Research and Training Programme (Grant Agreement No 101052200 — EUROfusion). Views and opinions expressed are however those of the author(s) only and do not necessarily reflect those of the European Union or the European Commission. Neither the European Union nor the European Commission can be held responsible for them. Author R.A. Tinguely supported by US DOE Grant DE-SC0014264.

References

[1] M.N. Rosenbluth, P.H. Rutherford, Phys. Rev. Lett. **34** (1975) 1428;

[2] A.B. Mikhailovskii, Sov. Phys. JETP **41** (1975) 890;

[3] A Fasoli *et al*. Progress in the ITER Physics Basis Chapter 5: Physics of energetic ions 2007 Nucl. Fusion **47** S264;

[4] A. Hasegawa and L. Chen, Phys. Rev. Lett. **32** (1974) 454 ;

[5] D.W. Ross *et al*. Phys. Fluids **25** (1982) 652;

[6] K. Appert *et al*. Plasma Phys. **24** (1982) 1147;

[7] C. Z. Cheng, L. Chen, and M. S. Chance, Annals of Physics **161**(1985) 21;

[8] G. Y. Fu and J. W. V. Dam, Phys. Fluids **B1** (1989) 2404;

[9] R. L. Dewar *et al.* Phys. Fluids **17** (1974) 930;

[10] R. Betti and J. P. Freidberg, Phys. Fluids **B3** (1991) 1865;

[11] S.E. Sharapov *et al*. Phys. of Plasmas **9** (2002) 2027;

[12] V.G. Kiptily *et al*. Plasma Phys. Control. Fusion **64** (2022) 064001;

[13] M. Fitzgerald *et al* 2023 Stability analysis of alpha driven toroidal Alfvén eigenmodes observed in JET deuterium-tritium internal transport barrier plasmas accepted for publication in *Nuclear Fusion*;

[14] V.A. Yavorskij *et al*. Phys. Plasmas **6** (1999) 3853;

[15] V.G. Kiptily *et al.* Nucl. Fusion **49** (2009) 065030;

[16] S.E. Sharapov *et al*. Fusion Sci. Tech. **53** (2008) 989;

[17] F. Clairet *et al.* Nucl. Fusion **56** (2016) 126019;

[18] J. Mlynar *et al*. Fusion Eng. Design **96** (2015) 869;

[19] V.G. Kiptily private communication (2023);

[20] Ž. Štancar *et al* 2023 Overview of interpretive modelling of fusion performance in JET DTE2 discharges with TRANSP, submitted to *Nuclear Fusion*;

[21] P. Batistoni *et al.* Nucl. Fusion **58** (2018) 106016;

[22] G. T. A. Huysmans, J. P. Goedbloed, and W. Kerner. Int. J. Modern Physics **C02** (1991) 371;

[23] S. Poedts and E. Schwartz, J. Comput. Phys. **105** (1993) 165;

[24] A.B. Mikhailovskii, G.T.A. Huysmans, W.O.K. Kerner, and S.E. Sharapov. Plasma Phys. Rep. 23 (1997) 844;

[25] H.J.C. Oliver *et al* 2023 Toroidal Alfvén eigenmodes observed in low power JET deuterium-tritium plasmas, accepted for publiucation in Nuclear Fusion;

[26] J. W. Connor, R. O. Dendy, R. J. Hastie, D. Borba, G. Huysmans, W. Kener, and S. Sharapov. *Non-ideal Effects on Toroidal Alfvén Eigenmode Stability*. In: Proceed. of 21st EPS Conf., vol. **18B**, page 616 (1994).